



12th Deep Sea Offshore Wind R&D Conference, EERA DeepWind'2015

Lagrangian Measurement of Waves and Near Surface Turbulence from Acoustic Instruments

Mostafa Bakhoday Paskyabi^{1,2}, Helge Thomas Bryhni¹, Joachim Reuder^{1,2}, Ilker Fer^{1,2}

*1 Geophysical Institute, University of Bergen, Norway
2 Bjerknes Center for Climate Research, Bergen, Norway*

Abstract

We demonstrate high-resolution measurements of upper ocean flow and turbulence using a Lagrangian drifter. A spherical buoy as a quasi-wave following drifter mitigate the contaminations induced by wave orbital velocities and motion-induced disturbances. The platform, with dimensions of 1.13 m diameter and 4.30 m overall length, is modified to include an Acoustic Doppler Velocimeter to measure time series of velocity fluctuations, a GPS logger, two GoPro video cameras to estimate both platform orientation and sea surface topography evolution, and a 5-beam Acoustic Doppler Current Profiler to collect near the surface velocity profiles. Results are reported from a 2-hour test deployment in November 2014, off Karmøy, Norway. This flexible measuring system is designed for a wide range of air-sea interaction studies, including the effect of wave breaking on the upper ocean variability. Such process understanding is of interest for the estimation of loads on fixed and floating offshore structures, and for efficient and optimal design of offshore platforms.

© 2015 The Authors. Published by Elsevier Ltd. This is an open access article under the CC BY-NC-ND license (<http://creativecommons.org/licenses/by-nc-nd/4.0/>).

Peer-review under responsibility of SINTEF Energi AS

Keywords: Lagrangian drifter; ADV; ADCP; Motion compensation; Wave-induced bias; Gravity waves; Structure functions; Inertial subrange.

1. Introduction

An efficient design of an offshore wind park to harvest optimal wind energy requires an accurate understanding of airflow, surface waves, and ocean currents, as well as their interaction with the wind turbines at the potential locations [1,2]. A large number of laboratory experiments, numerical simulations, and field observations has shown that turbulent fluctuations (including wake vortices) on both sides of wavy air-sea interface play an essential role for predictions of the flow affecting the turbines, fatigue loads and potential damages, lifespan of offshore installations, and the overall performance of the wind farm. In this investigation, we focus on obtaining a detailed

flow field understanding by conducting measurements near the sea surface using a Lagrangian drifter equipped with oceanographic and optical sensors.

Quality measurements of turbulent parameters near the sea surface have been hindered mainly due to: (1) the lack of stable oceanographic sensors to operate efficiently in the proximity of a wavy surface; and (2) the availability of appropriate processing methods to remove the surface wave-induced disturbances from the measured data. Recent progresses in development of sophisticated processing algorithms and advanced instruments have shown success in reducing or even removing the wave-biased contaminations from Eulerian measurements using acoustic-based instruments such as Acoustic Doppler Velocimeters (ADV) and Acoustic Doppler Current Profilers (ADCPs) mounted on offshore fixed platforms [3,4,5]. However, applications of the developed processing tools for the acoustic-based data are subject to some uncertainties and limitations: (1) In the variance method for turbulence measurements, even a small misalignment in hardware configurations or platform motions (or tilts greater than $\sim 2^\circ$) produces strong rotational wave covariance, which may result in erroneous measurements of Reynolds stresses; (2) in the structure function method, bin separations are limited to the scales in which turbulence remains isotropic; and (3) in the inertial dissipation method, an approximately broadband inertial subrange must exist in the measured velocity spectrum for determination of the dissipation rate of TKE. Consequently, Eulerian measurements of turbulent quantities exposed to energetic wave-induced variances, orders of magnitude larger than those associated with turbulence, are still a challenging issue and remain a relatively unexplored area of research in oceanography.

As a complement to Eulerian sensors, Lagrangian Instrumented Drifters (LIDs) appear to offer a good alternative for the measurements of turbulent quantities, particularly in close vicinity of the wavy air-sea interface [6]. Lagrangian sensors are able to measure local quantities in a turbulent flow with much lower noise levels in regions of active breaking crests, where the Eulerian sensors cannot operate efficiently. The geometry of sensors and their support structures significantly control the amount of such wave- and motion-induced noise levels resulting from generation of distorted flows and secondary turbulence surrounding the sensors' sampling volumes. While the LIDs offer a better spatial coverage relative to their Eulerian counterparts, the acquired data may reveal a non-stationary behavior even under fairly stationary wave conditions. As an example of such Lagrangian-measuring techniques, we refer to Thomson 2012 [6] who uses a surface wave instrument float with tracking to measure waves and dissipation rates of TKE in depths below 1.25 m. The dissipation rates are estimated based on the structure function of the velocity profiles acquired from a pulse-coherent Doppler profiler (Nortek Aquadopp) and from the inertial subrange method applied on point velocity measurements from an ADV.

In this study, the main objective is to report on a test deployment of a LID. The platform provides wave and turbulence measurements in a quasi-wave following reference frame near the sea surface. The onboard instruments consist of a down-looking Nortek Vector ADV and a profiling acoustic instrument (a Nortek 5-beam Signature 1000, Section 2.1). Additionally, a GoPro Hero3 Black digital camera was mounted on the top-side of a meteorological mast to directly observe the evolution of the sea surface topography. A second GoPro camera was attached to a bracket on the waterside. The short test cruise was carried out on November 2014, off Karmøy, Norway (Section 2.2 and Section 4). The collected data demonstrate the need for detailed investigations on the processing and interpretation of underlying processes to further assess the potential of LID for quality measurements of turbulent quantities (Section 3).

2. Measurements

2.1. Instruments

A spherical buoy (Flotation Tech.) was modified and used as a quasi-wave following drifter, with dimensions of approximately 1.13 m diameter and 4.30 m overall length (2.37 m draft and 1 m mast), suitable for use in both shallow and deep waters under different wind, wave, and current conditions. The lower frame (2.37 m draft) includes three attachment points for mounting the down-looking ADV, the 1000 kHz Nortek Signature 5-beam Doppler Profiler (henceforth, Nortek S1000), and a GoPro Hero3 Black camera with a slant angle of approximately 45° relative to the vertical. The drifter is extended about 1 m above the water surface (Fig. 1). This air-side

construction includes a GPS unit (in a waterproof box), and a self-powered GoPro digital camera attached on the top of the 1 m mast. The GPS sampled at 1 Hz, with a horizontal positioning accuracy of approximately 3 m. The drifter location is tracked in real time with a radio frequency transmitter. The Nortek S1000 was fitted to the water-side construction of the drifter with transducers situated approximately 120 cm below the center of the drifter with a grazing angle of 45° relative to the vertical. High-resolution (4 Hz temporal resolution) measurements of ocean velocity were recorded along the 5 beams using 10 cm bin sizes, ambiguity velocity of 0.01 ms^{-1} , and blanking distance of 0.6 m. The Nortek S1000 operated in burst mode, acquiring 15-minute data of every 16 minutes. In addition, a Nortek ADV was also fitted to the end of lower construction for independent single point velocity measurements. The down-looking Nortek ADV was set to sample at 8 Hz in a continuous data acquisition mode (Fig. 1-b).

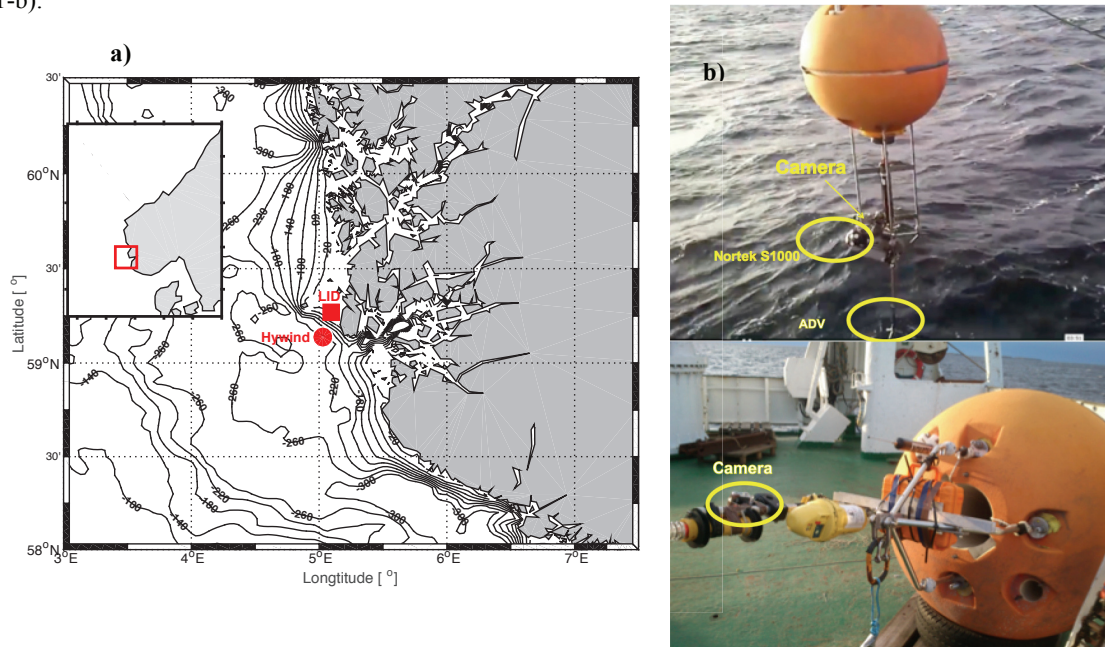


Fig. 1 (a) Map showing the deployment site (black square) and the location of the Hywind offshore floating wind turbine, off Karmøy, Norway. Isobaths are drawn at 50 m intervals. The inset shows the experiment site location in Norway; and (b) pictures of the Lagrangian Instrumented Drifter (LID) with the installed sensors indicated.

2.2. Site

Figure 1-a shows the experiment site and bathymetry. The measurements were made during a 2-day test cruise onboard R/V Håkon Mosby between 14 and 16 November 2014, and the LID deployment was carried out on November 16 from 9:44 to 11:20 UTC. The site is located on the west of the island of Karmøy, on the western Norwegian coast ($59^\circ 15.983' \text{ E}$, $5^\circ 7.639' \text{ N}$) at depths varying from 28 to 100 m along the trajectory of drifter. This site was selected because it is suited in the region of shallow water exposed to strong interaction between turbulent eddies, wave, and currents. Additionally, it is located in the close proximity of the 2.3 MW floating offshore wind turbine Hywind deployed and operated by Statoil.

Figure 2 provides a summary of wind, wave, and thermal conditions collected from the ship's meteorological mast at 15 m height above the mean sea level, and ADV's pressure data. Wind speed and direction were recorded every minute throughout the field campaign. Wind speed ranged from 0.5 to 12 m s^{-1} with directions predominantly from southeast (Fig. 2-a). During the LID experimental period, very energetic events occurred, characterized by an increase in wind speed together with a water temperature drop resulting in a temperature

difference of approximately 1°C between air and water (Fig. 2-b). Locally generated gravity waves are highly correlated with wind during the 2-hour deployment (departure from the old sea to the young sea, Fig. 2-c).

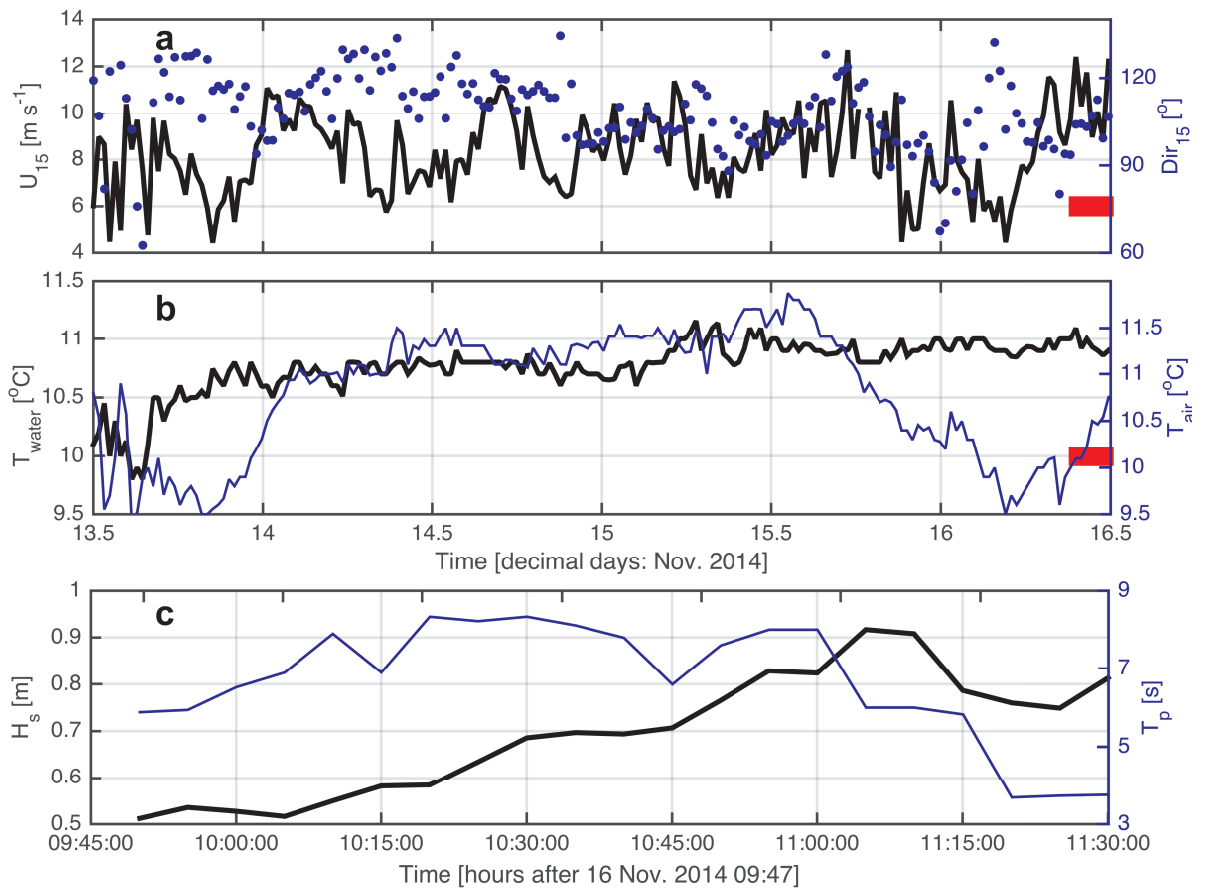


Fig. 2 Time series of (a) wind speed and direction at 15 m height collected from ship's meteorological mast. Wind direction is positive and clockwise from north; (b) air temperature measured at 15 m height (black) and water temperature (blue); and (c) the significant wave height and wave peak period measured from the ADV pressure signal after applying motion compensation during 2 hours deployment of LID. The horizontal red bars in Figs. 2-a and b indicate the relative duration of the LID deployment.

3. Background

Let $\mathbf{u} = (u, v, w)$ denote a velocity vector in a Cartesian coordinate frame (x, y, z) in which x , y , and z are axes along the mean flow direction, horizontally across the mean flow direction, and the vertical, respectively. The ambient flow is decomposed into the mean (overbar), wave (tilde), and fluctuating (prime) components such that:

$$\mathbf{u} = \bar{\mathbf{u}} + \tilde{\mathbf{u}} + \mathbf{u}'.$$

This separation is based on the assumption that there exist spectral gaps between mean flow, wave, and turbulence. However, this assumption is not always practical and gets violated due to the intermittent and random nature of gravity waves and turbulent motions. We further assume that flow is steady, horizontally homogeneous, and neutrally stratified. Under these conditions, neglecting the transport of TKE, and assuming a constant surface mechanical stress, the production of TKE is balanced by dissipation rate of TKE, ε :

$$\varepsilon = \frac{u_{*w}^3}{\kappa z}, \quad (1)$$

where u_{*w} denotes the water-side friction velocity, z is depth from the sea surface, and κ is the von Kármán constant. This section gives a brief overview of calculation of ε from the acoustic-based instruments mounted on LID.

3.1. Dissipation measurements using the ADV

ADVs measure the relative current velocity using the Doppler phase shift. Therefore, the quality of acquired velocity data depends directly upon the characteristics of the sound scattering in the water. Although, these point measuring techniques provide very high spatial focus with lower Doppler noise compared with profiling instruments, i.e. ADCPs, they are sensitive to phase wrapping. The phase wrapping occurs when the ambient flow exceeds a preprogrammed measurable velocity range. Another important drawback of using ADVs is that they cannot measure appropriately high-resolution currents when exposed to platform motions. This occurs in our application where the ADV is mounted on the Lagrangian drifter. In such situations, the relative water velocity and the ADV orientation (and motions) must be used to compensate for the motion-induced disturbances. Performing the motion correction requires accurate knowledge of the ADV orientations and motions which are provided by inertial motion sensors synchronous with each measured velocity data [1]. The ADV is equipped with an Inertial Motion Unit (IMU) with 3-axis accelerometer, gyroscope, and a magnetometer.

Once the velocity data are processed to remove the vast majority of intrinsic and extrinsic disturbances, the corrected velocity fluctuations can be used to determine the dissipation rate of TKE. By assuming that there exists an inertial subrange in the frequency spectrum of the acquired velocity time series, a one-dimensional universal spectrum can be applied to the inertial subrange as follows:

$$\phi_{ii}(f) = \frac{U_d}{2\pi} \alpha_i \varepsilon^{2/3} \left(\frac{2\pi f}{U_d} \right)^{-5/3}, \quad (2)$$

where $\phi_{ii}(f)$ denotes the frequency spectral density of the i th ($i = 1,2,3$) velocity component at the frequency f , and α_i is the Kolmogorov constant; $\alpha_1 = 0.51$ for locally isotropic turbulence [5]. Near the sea surface, U_d represents a non-turbulent drift velocity comprising of contributions from the mean flow, lower frequency oscillations, and gravity wave orbital velocities. Note that using Eq. (2) requires a steady drift velocity, the violation of which will distort the universal shape. This assumption whereby turbulent eddies are advected by the drift velocity is called Taylor's frozen turbulence hypothesis that may not be satisfied under the influence of strong shear flow, in particular in the close vicinity of the sea surface. Evolution and decay of breaking and non-breaking waves may further result in large wave-induced nonuniformity in the total advection velocity characteristics relative to the most energetic turbulent eddies. Although many studies of dissipation rate extraction from ADV near the sea surface have been conducted, satisfying the Taylor hypothesis underneath a moving and random interface is still a challenging topic.

3.2. Dissipation measurements from the ADCP

Similar to ADVs, ADCPs estimate the flow speed by measuring the Doppler frequency shift of acoustic pulses along different beams over a set of spatial bins. ADCPs use much larger sampling volume compared to the ADVs, to estimate the three components of the relative flow velocity along each beam (in a fixed coordinate frame). The sizes of these along-beam sampling volumes increase substantially as a function of distance from the transducer probe which corresponds to an imperfect spatial localization, higher the Doppler noise, and substantial decrease of the measurement accuracy [3].

In LID, a Nortek S1000 was mounted approximately 120 cm below the center of drifter with a slant angle of 45° with respect to the vertical. Along-beam velocities from the 5 transducers of Nortek S1000 exhibit energetic contribution from the surface gravity waves causing problem for estimation of turbulence energy spectrum (Eq. 2) and the Reynolds stresses. Several studies have been conducted to remove these wave-induced biases from the

measured velocity components. As an example, Wipple et al [4] used linear wave theory to separate the wave signal from the ADCP-based Reynolds stresses. Although their method is capable of isolating Reynolds stress estimates in mild wave conditions, the method cannot remove the wave-biased contamination under energetic waves. It should be noted that even small beam misalignments and instrument orientation errors can generate large wave-induced disturbances that can dominate the turbulent Reynolds stresses. Therefore, the motion-induced contaminations should be compensated by using an IMU (including an accelerometer, a gyroscope, and a magnetometer) before starting the wave-correction procedure.

A detailed analysis of the determination of Reynolds stresses in the presence of surface gravity waves can be found in [4]; we summarize here the general methodology for measuring horizontal Reynolds stresses from an up-looking Nortek S1000 using the variance method applied to 4 slanted beams (the 5th beam is vertical). Let u_1, u_2, u_3 and u_4 denote the four along-beam velocities. Using Eq. (1) and a beam deviation angle from the vertical θ , the variances of along beam velocities will satisfy the following expressions [7]:

$$\overline{u'w'} = \frac{(u'_3 + \tilde{u}_3)^2 - (u'_4 + \tilde{u}_4)^2}{4 \sin \theta \cos \theta} \quad \text{and} \quad \overline{v'w'} = \frac{(u'_1 + \tilde{u}_1)^2 - (u'_2 + \tilde{u}_2)^2}{4 \sin \theta \cos \theta},$$

where $\overline{u'w'}$ and $\overline{v'w'}$ are horizontal Reynolds stresses under the influence of surface gravity waves. Although these stresses suggest two different types of wave-induced contaminations, we focus only on wave-biased correction that relies on subtraction of wave-induced velocity components along each beam by the use of linear wave theory. This procedure leads to a substantial reduction of turbulent energy provided that a wave-induced attenuation parameter, which is assumed invariant, can be assigned accurately.

The TKE dissipation rates along each beam can also be estimated using the second-order structure function method by assuming locally isotropic turbulence hypothesis [6,8].

4. Results

The continuous time series from the ADV were parsed into 5-minute segments after applying quality control procedures to remove low pulse correlation and spikes. Wave orbital velocity contributions should be accounted for in the quality control procedures; however, here we present the quality-controlled ADV spectra with no wave orbital velocity isolation to highlight the elevation of variance by surface gravity waves, in particular in the inertial frequency band (Fig. 3). While it is expected to achieve better stationary behaviour from 5-minute bursts, the results are sensitive to the length of burst segments (we compared results over longer and shorter segments before choosing the 5-minute burst in our analysis). In order to give an indication of the wave-biased contaminations in the measured ADV signals, Fig. 3-a illustrates the representative velocity spectra. The spectrum for each velocity component is calculated using 128 s, 50% Hanning overlapped windows. At frequencies beyond the gravity wave peak, the vertical velocity spectrum exhibits a significant energy elevation which is perfectly correlated to the vertical component of accelerometer signal (Fig. 3-b). The accelerometer signals are then utilized to correct the contaminations appeared in the vertical velocity spectrum (Fig. 1-a, green curve). It is further shown that the platform's vibrations are extended both at high frequencies and at the frequencies covering the gravity wave frequency band. LID orientation spectra also demonstrates elevated energy levels at the wave-affected frequency band (Fig. 3-c). These spectra are not able to provide quantitatively accurate measurements of turbulence, and indicate that an accurate analysis requires the use of longer bursts together with sensing and removing wave-correlated sensor motions in order to estimate both gravity waves and to measure the turbulent Reynolds stresses.

Fig. 3-d shows the ADV measured pressure spectrum. Whilst we can apply directly the linear wave theory to compute the sea surface elevation and other wave bulk parameters, obtaining wave information requires the integration of the pressure data with levelled acceleration signals. Additional information regarding the motion compensation of pressure data can be found in [9,10].

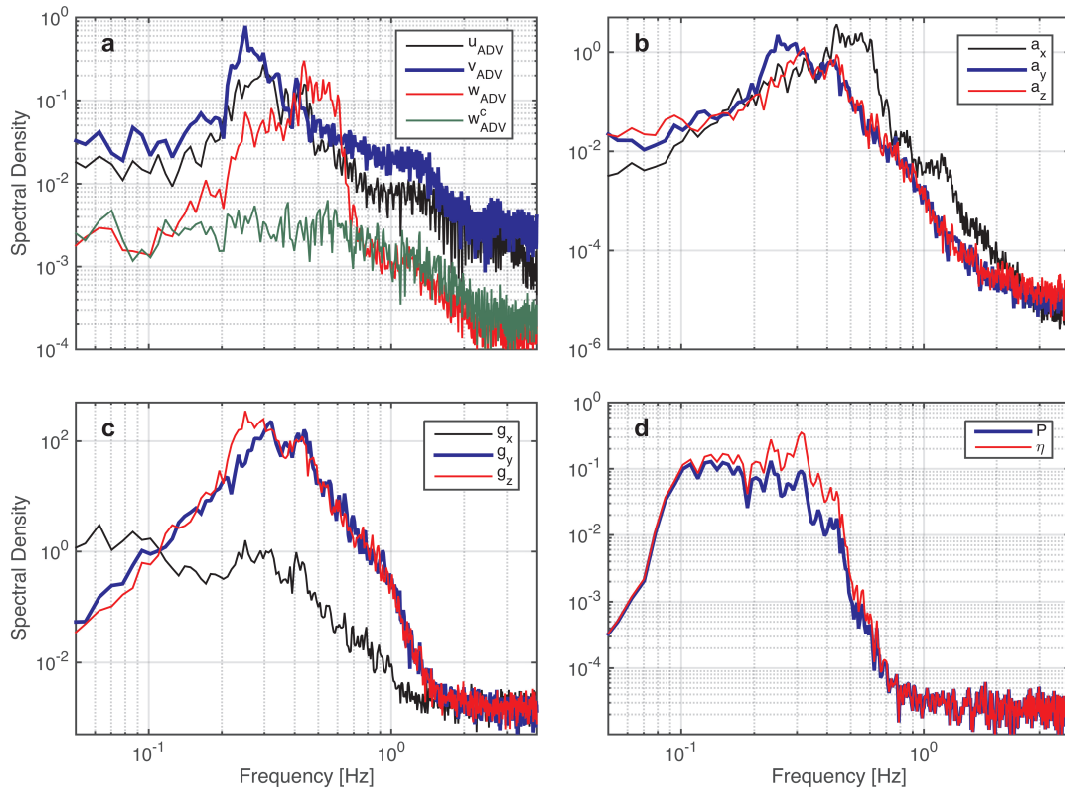


Fig. 3 Frequency spectra of (a) the three velocity components measured by the ADV for a 5-minute burst, The green curve shows the corrected vertical velocity spectrum using accelerometer signals; (b) the acceleration; (c) gyroscope signals from the IMU system; and (d) the pressure measured by the ADV pressure sensor for the same burst (blue). The sea surface elevation, η , is measured from the motion-compensated pressure data using the linear wave theory (red) [9,10].

Figure 4 shows the time series of atmospheric friction velocity over two-day period of the whole campaign (on November 14-16, 2014) at the experiment site. Bulk formulae were used to calculate the atmospheric momentum fluxes and air-side friction velocity [9]. Another independent estimate of u_{*a} from Eq. (3) and ADV velocity data is also presented in this figure from:

$$u_{*a}^{ADV} = \left(\frac{\phi_{33}(f)f^{5/3}}{\alpha_3} \right)^{1/2} \left(\frac{2\pi\kappa z}{U_d} \right)^{1/3}, \quad (3)$$

where $\alpha_3=0.68$, and z is the depth of the ADV sampling volume. For the stationary drift speed necessary for the Taylor's frozen turbulence hypothesis, we use the root-mean-squared velocity relying on the assumption that at each ADV burst, the velocities are stationary. The comparison shows discrepancy between the two estimates of u_{*a} (by a factor of 8) mainly because of the biases induced by the energetic gravity waves (see Section 3.1).

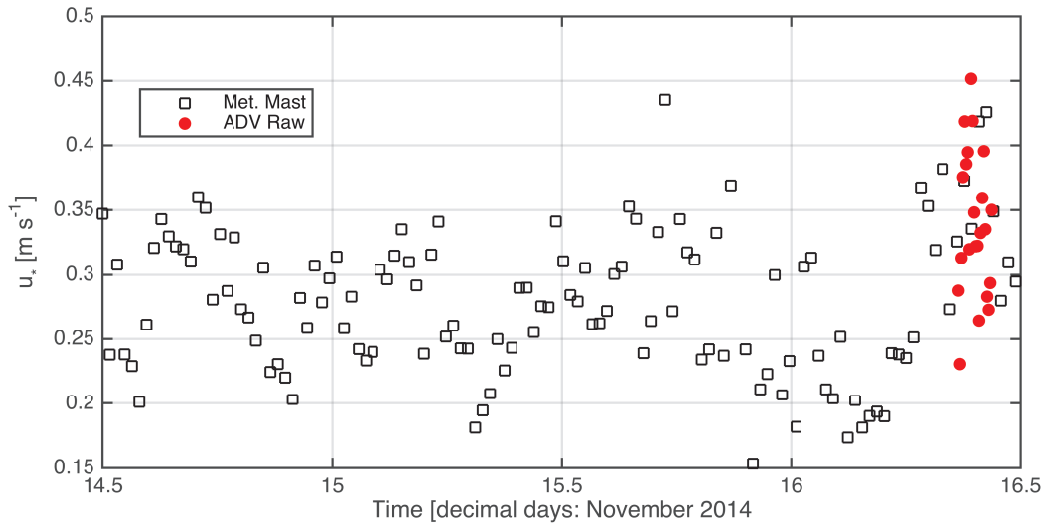


Fig. 4 Comparison between time series of measured airside friction velocity from wind speed at 10 m height (black squares) and those estimated from ADV measurements (Eq. 3, red markers) that have been scaled by a factor of 8 for the sake of better representation.

Data from the Nortek S1000 are initially screened for poorly correlated beams and bad data. The low correlated beams are then flagged as poor quality data and removed by linear interpolation. Figure 5-a and c show the 1-minute segments of contoured velocity data along 1 and 3 beam axes under the influence of gravity waves, after accurate determination of sea surface. A comparison between range-averaged velocity cospectra in the 1-3 and 2-4 directions is shown in Figs. 5-b and d. The beam-based Reynolds stresses demonstrate apparent covariance in the wave-affected frequency band in which the wave orbital velocities are orders of magnitude greater than the turbulent fluctuating velocities. To check this, we utilize the linear wave theory [10], and estimate the pressure-based vertical velocity spectra, S_{ww} , as a reliable indicator for the wave-induced energy elevation (Fig. 5-d). The high correlation between the bin-averaged 1-3 and 2-4 axes velocity spectra and S_{ww} confirms the substantial wave-induced errors in the near surface measurements of turbulent fluxes.

Figure 6 shows the velocity measurements from the vertical beam at 4 levels. At upper levels (close to the sea surface), a coherent wave pattern is seen across the inertial subrange frequency band, and turbulent patches are distributed almost everywhere. Figure 6-a illustrates further the appearance of small-scale oscillations correlated with the support structure motions. We observe a flattening of the vertical velocity spectrum for bins close to the sea surface as a result of extension of wave disturbances over a broad range of scales even greater than the wave spectral peak. The slopes of the spectra beyond the wave-affected frequency range depend strongly on the strength of turbulent coherent structures. One major problem with measurements underneath an energetic wave field is the overestimation of TKE and its dissipation rate, because most of the velocity spectra may not adhere to a slope of $-5/3$.

To improve the processing of measured data, we apply a spectral decomposition technique to reduce the contributions due to the unwanted motion-related disturbances [7]. Of particular interest is the corrected energy content, localized about the motion-related frequency band, which may be thought of as either random gravity waves or organized body vibrations. While this decomposition of turbulent and body motion scales exhibits an inertial subrange with approximately a $-5/3$ slope, the method may fail in the presence of energetic surface waves which tend to mask the turbulent levels throughout the inertial subrange. An accurate account of motion compensation and decomposition of turbulence from the mean field using the IMU data is outside the scope of the present work and will be reported elsewhere.

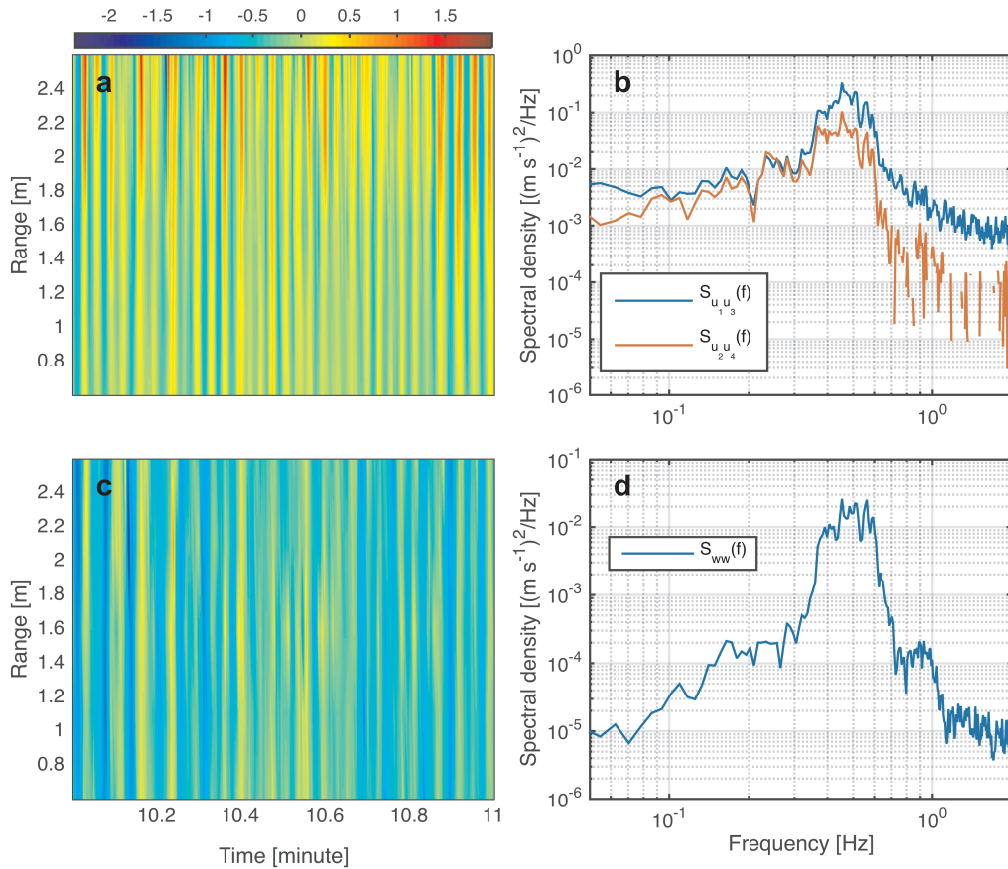


Fig. 5 (a,c) Time-depth evolution of velocities along 1 and 3 directions measured by the Nortek S1000 over one minute. (b) the bin-averaged velocity cospectra from 1-3 axis ($S_{u_1 u_3}$) and 2-4 axis ($S_{u_2 u_4}$); and (d) pressure-based vertical velocity spectrum, S_{ww} .

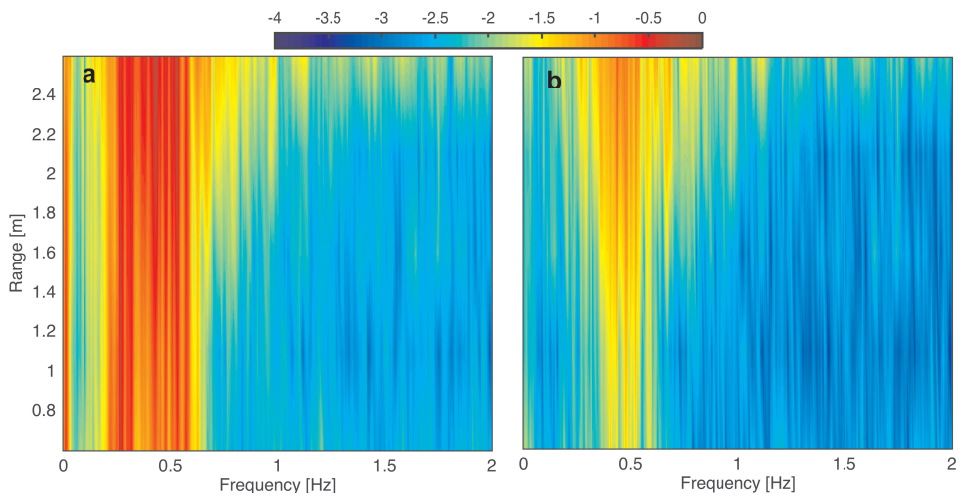


Fig. 6 (a) Vertical velocity spectra at different depth levels extracted from the Nortek S1000 vertical beam for a 5-minute burst with a sampling frequency of 4 Hz; and (b) the same burst spectra after applying the motion-filtering algorithm.

5. Conclusions

We present a short-term test deployment of a Lagrangian Instrumented Drifter (LID) which shows the potential to measure surface gravity waves, high-resolution currents, and turbulent fluxes near the sea surface in the presence of surface gravity waves. The platform moves and rotates in response to the wind, wave, and current induced motions. The measured data are not only affected by platform motions and its mechanical vibrations but also by the orbital motions of gravity waves, as well as turbulence generated by the support structure itself. We showed the physics of the motion-turbulence and the wave-turbulence interactions from acoustic instruments (i.e. single point and profiling) mounted on the LID. The shape of the velocity spectra consists of an energy-elevated portion in which gravity waves occupy the same frequency range as turbulence. However, energy spectra at higher frequencies are not fully free of contaminations induced by waves, and turbulent levels poorly exhibit a slope of $-5/3$ across the transient frequency band of the inertial subrange. This results in an overestimation of dissipation rates of turbulent kinetic energy.

We further tested a Nortek 5-beam Signature mounted on the LID, with a slant angle of 45° looking to the sea surface, to measure high-resolution current profile near the sea surface. Movements and orientation of the supporting buoy induced relative velocity components to the measured velocity data in beam coordinate frame on a broad range of frequencies. We implemented a decomposition algorithm to reduce these motion-induced contaminations by mitigating the elevated energy components in the wave-affected subrange. The combination of platform motions, instrument Doppler noise, limitations related to spatial resolution, and the assumption of spatially homogeneous flow yield ADCP velocity spectra of lesser quality compared with those obtained from the ADV.

Acknowledgements

This work has been performed as part of the Norwegian Center for Offshore Wind Energy (NORCOWE) funded by the Research Council of Norway (RCN 1938211560). Part of the instrumentations has been provided by the OBLO (Offshore Boundary Layer Observatory) project (RCN: 227777). Additional funding was also provided by the Prediction and Observation of the Marine Environment (POME) exchange program. We also express our gratitude to Martin Flügge (CMR/AS) for his kind help and support during the cruise.

References

- [1] Bakhoday-Paskyabi M, Flügge M, Edson JB, Reuder J. Wave-induced characteristics of atmospheric turbulence flux measurements. *Energy Procedia*, 2013, 25, 102-112.
- [2] Bakhoday-Paskyabi M, Fer I. Upper Ocean Response to Large Wind Farm Effect in the Presence of Surface Gravity Waves, *Energy Procedia*, 2012, 24, 245-254.
- [3] Rippeth, TP, Williams E, Simpson, JH. Reynolds stress and turbulent energy production in a tidal channel, *J. Phys. Oceanogr.*, 2002, 32, 1242-1251.
- [4] Whipple AC, Luettich, RA, Seim, HE. Measurements of Reynolds stress in a wind-driven lagoonal estuary, *Ocean Dynam.*, 2006, 56, 169–185.
- [5] Trowbridge J, Elgar S. Spatial scales of stress-carrying nearshore turbulence. *J. Phys. Oceanogr.*, 2003, 33, 1122–1128.
- [6] Thomson J. Wave breaking dissipation observed with SWIFT drifters, *J. Atmos. Oceanic Technol.*, 2012, 29(12), 1866–1882.
- [7] Lu Y, Lueck RG, Huang D. Turbulence characteristics in a tidal channel. *J. Phys. Oceanogr.*, 2000, 30, 855–867.
- [8] Wiles PJ, Rippeth TP, Simpson JH, Hendricks PJ. A novel technique for measuring the rate of turbulent dissipation in the marine environment. *Geophys. Res. Lett.*, 2006, 33, L21608.
- [9] Bakhoday-Paskyabi M. Small-scale turbulence dynamics under sea surface gravity waves, PhD thesis, University of Bergen, 2014, <http://hdl.handle.net/1956/8692>
- [10] Bakhoday-Paskyabi M, Fer I. Turbulence structure in the upper ocean: a comparative study of observations and modeling, *Ocean Dyn.*, 2014, 64, 611-631.